ELSEVIER
Journal of Biomechanics 41 (2008) 2312–2318
JOURNAL OF BIOMECHANICS
www.elsevier.com/locate/jbiomech
www.JBiomech.com

The effect of shape on the margination dynamics of non-neutrally buoyant particles in two-dimensional shear flows

F. Gentile[a,b], C. Chiappini[d], D. Fine[d], R.C. Bhavane[b], M.S. Peluccio[b,e], M. Ming-Cheng Cheng[b], X. Liu[b], M. Ferrari[b,f], P. Decuzzi[a,b,c,*]

[a]*BioNEM—Center of Bio-/Nanotechnology and-/Engineering for Medicine, University of Magna Graecia at Catanzaro, Viale Europa, Loc. Germaneto, 88100 Catanzaro, Italy*
[b]*The University of Texas Health Science Center, 1825 Pressler, Suite 537D, Houston, TX 77031, USA*
[c]*CEMEC—Center of Excellence in Computational Mechanics, Politecnico di Bari, Via Re David 200, Bari, Italy*
[d]*The University of Texas at Austin, 1 University Station, Austin, TX 78712, USA*
[e]*Dipartimento di Meccanica, Politecnico di Torino, C.so Duca degli Abruzzi 24, 10129 Torino, Italy*
[f]*M.D. Anderson Cancer Center and Rice University, Houston, TX 77030, USA*

Accepted 23 March 2008

Abstract

The margination dynamics of microparticles with different shapes has been analyzed within a laminar flow mimicking the hydrodynamic conditions in the microcirculation. Silica spherical particles, quasi-hemispherical and discoidal silicon particles have been perfused in a parallel plate flow chamber. The effect of the shape and density on their margination propensity has been investigated at different physiologically relevant shear rates S. Simple scaling laws have been derived showing that the number n of marginating particles scales as $S^{-0.63}$ for the spheres; $S^{-0.85}$ for discoidal and S^{-1} for quasi-hemispherical particles, regardless of their density and size. Within the range considered for the shear rate, discoidal particles marginate in a larger number compared to quasi-hemispherical and spherical particles. These results may be of interest in drug delivery and bio-imaging applications, where particles are expected to drift towards and interact with the walls of the blood vessels.

Keywords: Particle dynamics; Sedimentation; Fluidic chamber; Drug delivery

1. Introduction

The intravascular delivery of nanoparticles for biomedical imaging and therapy is being recognized as a powerful and promising tool in cardiovascular and oncological applications (LaVan et al., 2003; Ferrari, 2005a, b). Nanoparticles can be loaded with drug molecules and contrast agents and transported by the blood flow through the circulatory system. They are generally decorated with ligand molecules which are able to interact specifically with antigens expressed over diseased cells (target cells), which could be cells lining the blood vessels (vascular targeting) or cells in the extravascular space.

The power of nanoparticles over freely administrated drug molecules or imaging tracers relies on their multifunctionality and engineerability. As regarding multifunctionality, a nanoparticle can carry several hundreds of thousands of drug molecules and imaging agents increasing dramatically the drug dose released locally over time and the imaging contrast too. Different drug molecules can be loaded and released with a precise time schedule at the same location allowing for complex multidrug therapies. But even more important than multifunctionality is the engineerability of the nanoparticles. In fact, differently from drug molecules, nanoparticles are entities with defined geometrical, physical and chemical properties which can be controlled during the fabrication and

*Corresponding author at: The University of Texas Health Science Center, 1825 Pressler, Suite 537D, Houston, TX 77031, USA.
Tel.: +1 713 500 3363; fax: +1 713 500 2462.
E-mail address: Paolo.Decuzzi@uth.tmc.edu (P. Decuzzi).

0021-9290/$ - see front matter © 2008 Elsevier Ltd. All rights reserved.
doi:10.1016/j.jbiomech.2008.03.021

synthesis process and provide superior particle performances (Decuzzi and Ferrari, 2006). Several different particles have been presented in the literature that may be used for both therapy and medical imaging, ranging in size from few tens of nanometers to hundreds of nanometers (Choi et al., 2005; Duncan, 2003; Crommelin and Schreier, 1994) and up to few microns (Cohen et al., 2003); with different shapes, from the classical sphere, to spheroids (van Dillen et al., 2004) and even more complex shapes (Rolland et al., 2005) and with different composition and chemico-physical properties.

An 'optimally' designed nanoparticle should be able to navigate into the circulatory system, recognize the diseased cells (biological target) with high selectivity and adhere firmly to them (Decuzzi and Ferrari, 2006). The recognition process not only relies on the specific and non-specific interactions originating at the particle/cell interface, but evidently requires also close proximity between the particle and the target cell. In other words, particles should be designed to drift laterally towards the vessel walls, as leukocytes during an inflammatory process, rather than moving within the core of the vessels, as red blood cells generally do in the macro- and micro-circulation. By doing so, a particle would have the ability of sensing the vessel walls for biological and biophysical diversities, such as the overexpression of specific antigens (Neri and Bicknell, 2005) which could be used as 'docking site' in vascular targeting, or the presence of openings and fenestrations (di Tomaso et al., 2005) through which sufficiently small particles can cross the endothelial barrier.

The margination of leukocytes, at sites of inflammation, is an active process accompanied by a localized dilatation of the vessels and a decrease in blood flow velocity, and possibly favored by the interaction with the red blood cells which accumulating within the core of the vessels tend to push the leukocytes towards the periphery (Goldsmith and Spain, 1984). Nanoparticles used in biomedical applications are at least one order of magnitude smaller than red blood cells and leukocytes, therefore their margination cannot rely on such a mechanism. The shape and the density of the particles can be tailored to affect their margination propensity: spherical particles in a capillary flow would drift towards the vessel walls if and only if they are subjected to an external force field (Decuzzi et al., 2005); non-neutrally bouyant spherical particles have been observed and are predicted to drift laterally both in horizontal and vertical capillaries (see Hogg, 1994 and references there in); non-spherical particles exhibit a fairly complex dynamics with tumbling and rolling motions (Gavze and Shapiro, 1998; Pozrikidis, 2006). In this paper, the margination dynamics of non-neutrally buoyant particles with different shapes (quasi-hemispherical and discoidal) within a capillary flow is studied and compared to the dynamics of classical spherical particles.

2. Materials and methods

2.1. The particles

The spherical particles were purchased from polysciences. They are uniform, plain non-porous silica (SiO_2) microspheres with a diameter of about 1 μm and a density $\rho = 2000\,kg/m^3$, as shown by the SEM image in Fig. 1. The solid polysilicon particles were fabricated starting with a cleaned silicon wafer. Then an 800 nm silicon dioxide film was deposited by using wet oxidation process; a 330 nm polysilicon film was deposited by LPCVD. Finally, the 1.5 μm circular particles were patterned all over the polysilicon film using a standard photolithography process. Reactive ion etching was applied to remove undesired areas, and after stripping the photoresist, the polysilicon particles were released by removing the silicon dioxide layer in HF solution. An SEM image of the particle is given in Fig. 1. The quasi-hemispherical particles are porous silicon particles with different diameters and densities ($\simeq$ 1400 and 1900 kg/m^3), obtained by controlling particle porosity during the manufacturing process. Heavily doped 4 in p++ type (1 0 0) wafer were made into porous silicon particles modifying the protocols described in Cohen et al. (2003) to attain extreme control over the key characteristics of the microparticles such as shape and pore morphology. High uniformity and reproducibility were observed through SEM micrographs of the particles taken over different wafers (Fig. 1). The larger particles were estimated having a 3.2 ± 0.1 μm diameter and 1.05 μm thickness while the smaller were estimated having a diameter 1.6 ± 0.1 μm and 0.86 μm thickness. The microparticles were oxidized to obtain a high degree of hydrophilicity.

2.2. The flow chamber system

The system is similar to that used by several groups for analyzing the dynamics of circulating blood cells (among many others Gopalan et al., 1997) and microparticles (Shinde Patil et al., 2001). It consists of a PMMA flow deck with inlet and outlet bores, a silicon rubber gasket and a 35 mm glass dish sandwiched together (Fig. 2) from GlycoTech Corporation. The channel, defined by the gasket, has a thickness h of 0.01 in (254 μm), a

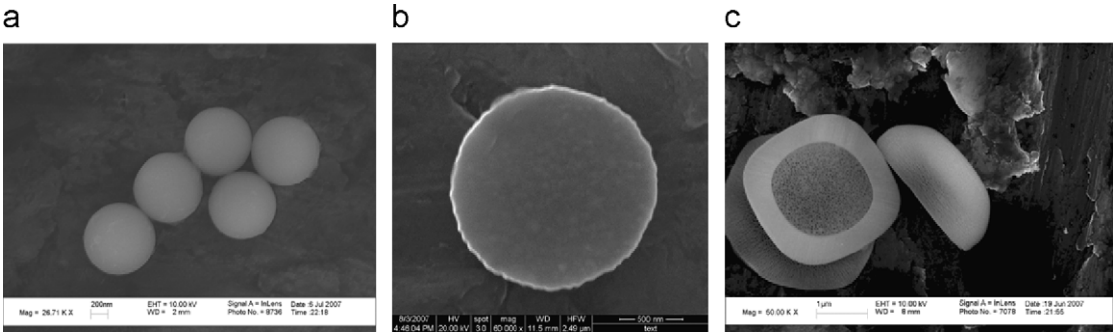

Fig. 1. SEM micrographs of spherical silica particles (1 μm solid particle), of discoidal polysilicon particles (1.5 μm × 0.3 μm solid particle), and of quasi-hemispherical silicon particles (3.2 μm porous particle).

length l of 2 cm and a width w of 1 cm. The inlet bore is connected to a syringe pump (Harvard Apparatus) through silastic tubing, and the outlet bore to a reservoir. In order to reduce the dead volume associated with the external tubing, the syringe pump has been located as close as possible to the flow chamber and tubings with the smallest internal diameter have been used for the connections (ID of about 1 mm).

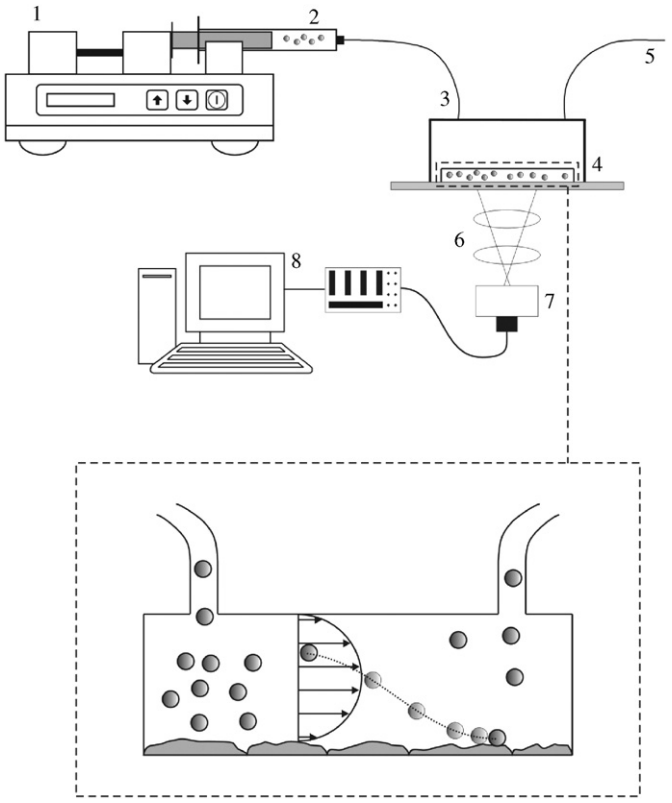

Fig. 2. A sketch of the experimental set-up comprising a syringe pump (1); a syringe with particles in solution (2); inlet silastic tubing (3); a parallel plate flow chamber (4), outlet silastic tubing (5); a microscope (6) with a digital camera (7) connected to a computer (8) for storage and imaging analysis.

The volumetric flow rate Q can be accurately controlled through the syringe pump and has been set equal to 32.258, 64.516, 129.032 and 322.58 μl/min, to generate shear rates S at the wall, respectively, of 5, 10, 20 and 50 s^{-1}, as derived by the relation

$$S = 6Q/h^2 w \tag{1}$$

used for such type of chambers. The maximum mean fluid velocity within the chamber is given by $U_{mean} = Q/(wh) \simeq 2$ mm/s, comparable with that estimated for the silastic tubing ($\simeq 7$ mm/s). And the Reynolds number is given by $Re = 2wh\rho U_{mean}/[(w+h)\mu] \simeq 1$, calculated considering the hydraulic diameter of the chamber $2wh/(w+h) \simeq 500$ μm, which is clearly associated with a laminar flow. Experiments were performed at room temperature (24 °C) for a maximum time of 20 min.

2.3. The glass dish coating

The glass cover slips used in these experiments have been coated using type I collagen from rat tail (Sigma-Aldrich). An initial solution with a concentration of 4 mg/ml has been diluted in DI water in order to obtain 10 μg/cm^2. Sterile cover slips have been kept at room temperature for an average period of 5 h and then let dry overnight.

2.4. The imaging system

The flow chamber was mounted on the stage of a Nikon Eclipse TE2000-E inverted microscope. The particle motion was observed using a 20× dry microscope objective, so that particles with a characteristic size of 1 μm or above were clearly visible using the bright field modality. The region of interest (ROI) of 276.48 × 276.48 μm^2 was mapped into 512 × 512 lines and conveyed to a computer for storage using a Nikon DQC-FS digital camera. For each experiment, depending on the flow rate, the acquisition rate was accurately tuned to allow for an adequate analysis of the dynamics of the particles. A suitable look up tables (LUTs) was applied to obtain the best contrast and brightness for the bright field images. These data were exported as tiff files into MatLab 6.5 (2002) and Mathematica (Wolfram, 2003) giving at each time period the image of the ROI with the particles.

2.5. The adhering particles

The number of adhering particles n at each time point was estimated by comparing pairs of consecutive frames in the time sequence and using an

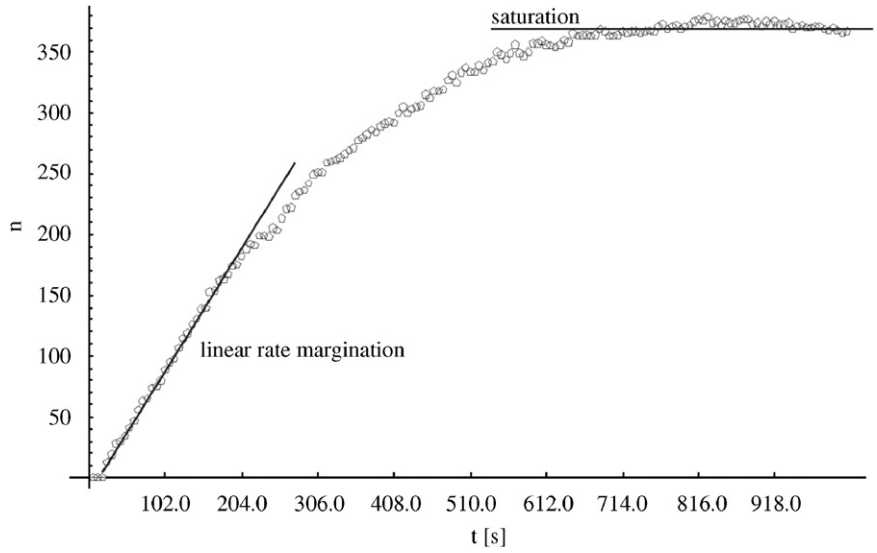

Fig. 3. The typical plot for the number of particles n marginating onto the substrate over time t.

ad hoc code developed in MatLAB/Mathematica. The number of particles adhering within the ROI were monitored for the whole duration of the experiment leading to characteristic curves as that show in Fig. 3 with an initial linear growth of n over time and a saturation towards the end of the experiment. The ROI was located for each experiment approximately in the mid of the chamber, sufficiently away from the lateral walls (25 times the characteristic size of the ROI) and from the inlet and outlet ports (50 times the characteristic size of the ROI), so to have a well-developed two-dimensional laminar flow.

All the experiments were performed holding constant the total number of particles injected into the channel being $n = 10^7$/ml, thus leading to a volume fraction of solids less than 0.3% for all type of particle considered. Particles were counted using a Z2 Coulter Particle Counter and Size Analyzer (Beckman Coulter, Fullerton, CA, USA). It should be noticed that, generally, the number of particles used in such experiments is of the order of 10^6/ml for both cells (Gopalan et al., 1997) and microparticles (Shinde Patil et al., 2001) adhesion assays. By working with such an excess of particles any possible effect of dead volumes within the apparatus on the accuracy of the experimental results can be neglected. In fact, consistently with what shown in Fig. 3, the number of adhering particles over the ROI has been of a few hundreds and similar values have been observed also over regions near the ROI. Thus assuming conservatively an uniform deposition of the particles over the whole substrate, the total number of adhering particles would have been of the order of 10^6, that is to say only 10% of the injected particles would adhere to the flow chamber substrate and 90% would be transported away from the flow.

3. Results and discussions

The number of particles n sedimenting and attaching to the collagen substrate within the ROI is shown in Figs. 4–7 as a function of the shear rate S for different particle types.

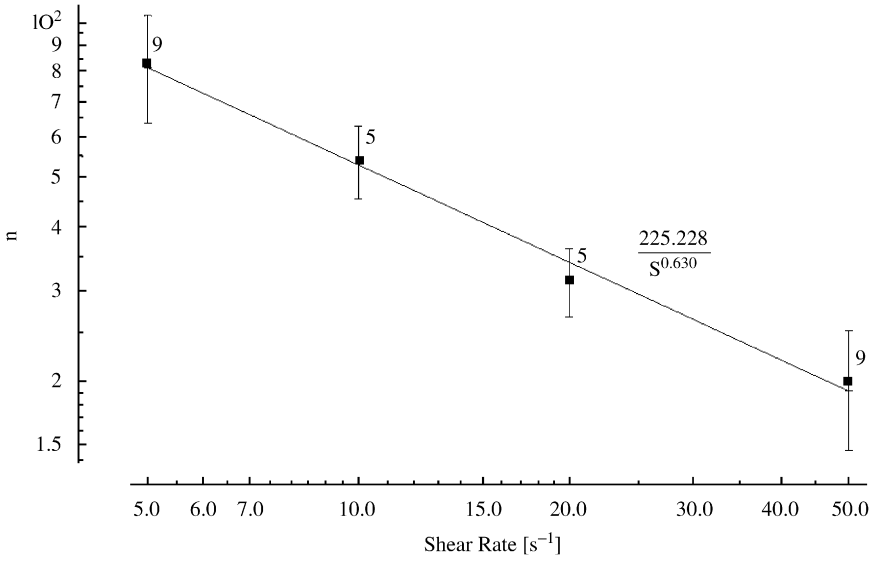

Fig. 4. The number of particles n marginating at the steady-state onto the substrate as a function of the shear rate S—spherical silicon 1 μm particles.

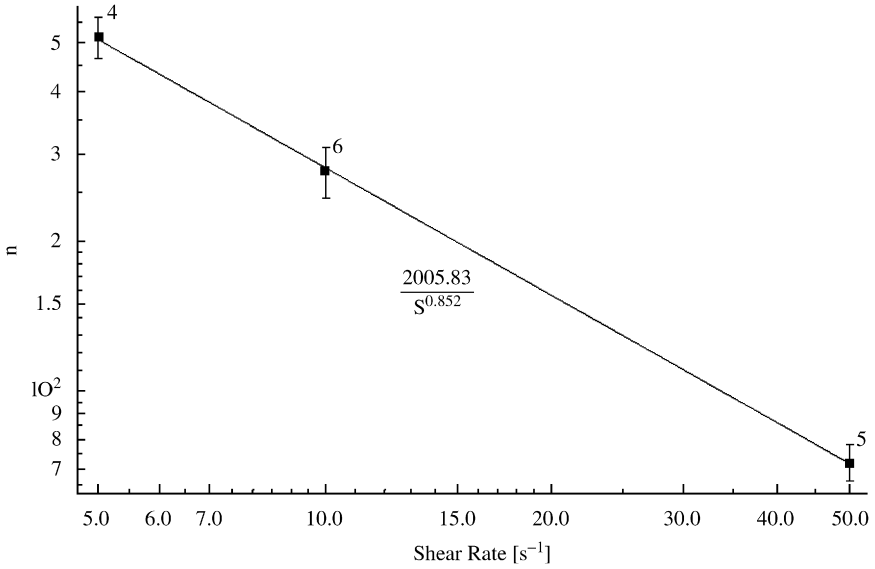

Fig. 5. The number of particles n marginating at the steady-state onto the substrate as a function of the shear rate S—discoidal polysilicon 1.5 μm × 0.3 μm particles.

The geometrical and physical properties of the particles which are of interest for this analysis are listed in Table 1.

In Fig. 4, spherical 1 μm solid (non-porous) silica particles with a density $\rho = 2000\,\mathrm{kg/m^3}$ are considered. The number of sedimenting particles reduces as the shear rate S increases, as expected since the 'time of flight' of the particles within the ROI reduces with S, and the $n-S$ relation is quite linear in a double logarithmic plot with a scaling law $n \simeq 225 \times S^{-0.63}$ and $R^2 = 0.989$.

In Fig. 5, the number of discoidal polysilicon particles with a diameter of 1.5 μm and a density of $\rho = 2200\,\mathrm{kg/m^3}$ are considered. The scaling law exponent derived for the $n-S$ is of about 0.85 with $R^2 = 0.999$, larger than what obtained for the spherical particles.

In Fig. 6, the number of quasi-hemispherical silicon particles with a 1.6 μm diameter sedimenting within the flow chamber is shown for large (LD) and small (SD) density particles. The SD particles have a density $\rho_{SD} \simeq 1360\,\mathrm{kg/m^3}$, whereas for the LD particles it is $\rho_{LD} \simeq 1840\,\mathrm{kg/m^3}$. For both particles, the relationship $n-S$ can be described by a line within a double logarithmic diagram and in particular it is $n_{LD} \simeq 1263 \times S^{-1.02}$ for the LD particles and $n_{SD} \simeq 498 \times S^{-1.13}$ for the SD particles, with $R^2 = 0.987$ and 0.998, respectively. Therefore regardless of the density of the particles, the scaling exponent is almost the same and close to unity; and the ratio between the numbers of sedimenting LD and SD particles is consistent with their density ratio being $n_{LD}/n_{SD} \simeq \frac{1263}{498} \simeq$

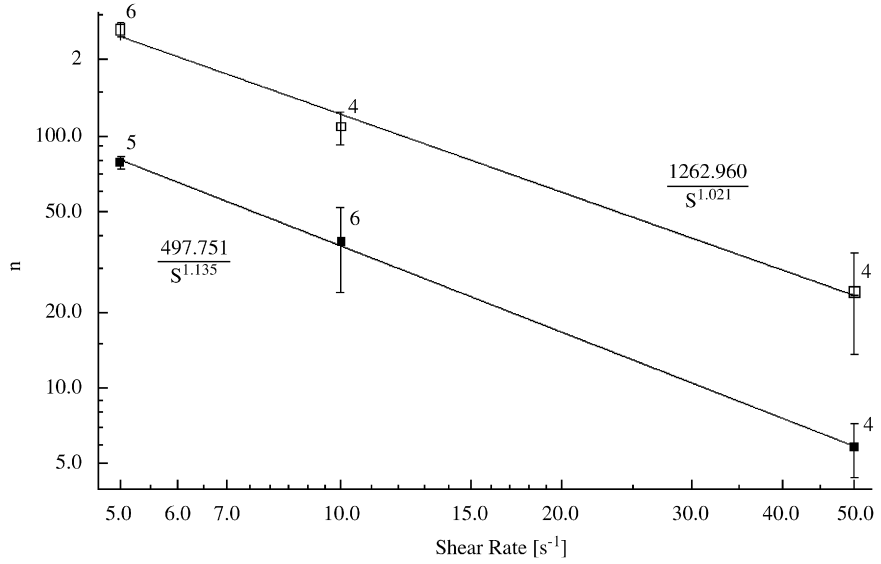

Fig. 6. The number of particles n marginating at the steady-state onto the substrate as a function of the shear rate S—quasi-hemispherical silicon 1.6 μm particles small pores (white boxes) and large pores (black boxes).

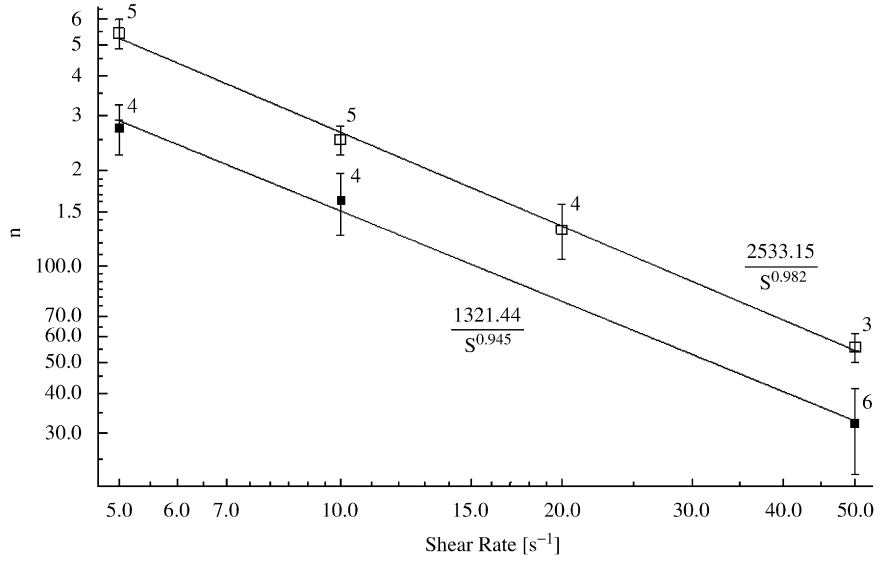

Fig. 7. The number of particles n marginating at the steady-state onto the substrate as a function of the shear rate S—quasi-hemispherical silicon 3.2 μm particles small pores (white boxes) and large pores (black boxes).

2.53 and $\rho_{LD}/\rho_{SD} \simeq 2.334$. Similar results have been obtained in the case of quasi-hemispherical particles with a diameter of 3.2 μm, as shown in Fig. 7. The scaling exponent for S is of the order of unity again even for these larger particles, namely $n_{LD} \simeq 2533 \times S^{-0.98}$ and $n_{SD} \simeq 1321 \times S^{-0.94}$, with $R^2 = 0.997$ and 0.993, respectively. And even in this case, the ratio between n_{LD} and n_{SD} is consistent with the density ratio being $n_{LD}/n_{SD} \simeq \frac{2553}{1321} \simeq 1.91$ and $\rho_{LD}/\rho_{SD} \simeq 2.34$. It is here very important to emphasize that neither a change in density (LD against SD) nor a change in size (1.6 μm against 3.2 μm) of the quasi-hemispherical particles has affected significantly the scaling exponent for the $n-S$ relationship which has been found to be close to unity. And it should then be associated to the shape of the particle more than to other properties.

The margination behavior of the three different particles is shown in Fig. 8, where a direct comparison with the absolute number n of sedimenting particles over the same ROI is shown. The discoidal particles are about 20% heavier than the spherical but the number of discoidal sedimenting particles is on the average 5 times larger, within the range of shear rates considered. On the other hand, the quasi-hemispherical particles are about 60% heavier than the spherical particles but the number of sedimenting particles is about 3 times larger at $5\,s^{-1}$ and just 20% larger at $50\,s^{-1}$.

Table 1

	Material	Size (μm)	Porosity	Volume (fl)	Mass (pg)
Sphere	SiO_2	1.0	Solid	0.58	1.28
Quasi-hemispherical	Si	1.6	Porous	$\simeq 0.75$	1.65
Discoidal	*p*-Si	1.5 × 0.3	Solid	0.52	1.04

The mass of the particles is slightly different, depending on the particle type as listed in Table 1, thus leading to slightly different gravitational forces being of about 12 fN for the discoidal, 16 fN for the quasi-hemispherical and 10 fN for the spherical particles. Whilst the gravitational force is fixed within the flow domain, the hydrodynamic and colloidal forces, as the van der Walls and electrostatic double layer interactions, do depend on the separation distance between the particle and the surface. Within the center of the chamber with a maximum velocity of the order of 1 mm/s, the classical Stokes relation ($3\pi\mu dU$) would predict a drag force of the order of 10 pN over a 1 μm spherical particle, and it would reduce to about 0.4 pN for the same particle adhering to the chamber substrate with a shear rate of $50\,s^{-1}$, as from $5/2\pi\mu d^2 S$ derived by Goldman et al. (1967). Similar values have been estimated for discoidal and hemispherical particles in a linear laminar flow bounded by a rigid wall (Lee and Decuzzi, 2008). Colloidal forces would have comparable values only for particle/substrate separation distances smaller or at most comparable with the size of the particle (i.e. 1 μm), and would then be of importance only at the very end of the margination process, as observed by Decuzzi et al. (2005). Therefore, despite their small values, the generalized hydrodynamic forces (drag, lift and torque) exerted over the particles dominate and govern their margination dynamics, whereas colloidal forces would be of equal importance only in close proximity with the vessel walls, that is to say at the end of the margination process.

4. Conclusions

Using a parallel plate flow chamber mimicking the hydrodynamic conditions in the microcirculation, the effect

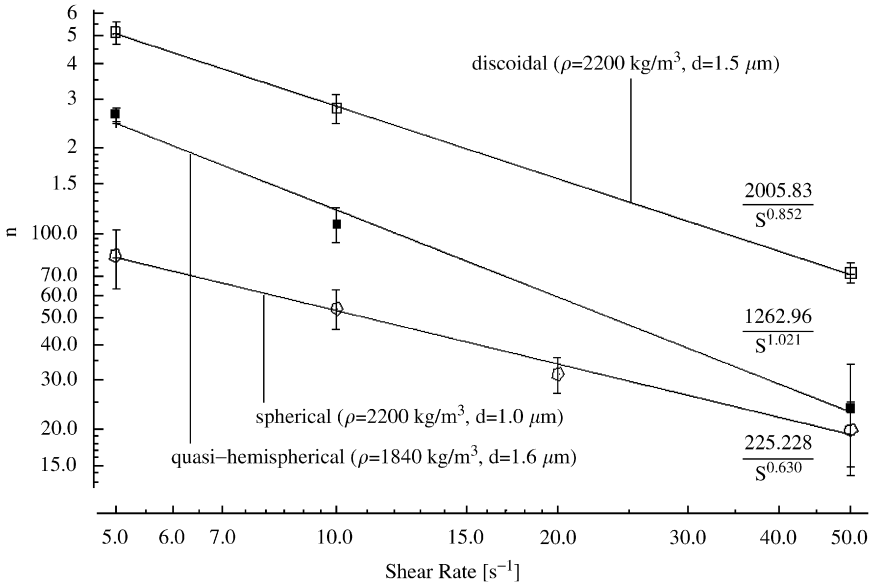

Fig. 8. A comparison among the $n-S$ scaling laws for silica spherical (white pentagons), discoidal polysilicon (white boxes) and 1.6 μm silicon quasi-hemispherical particles (black boxes).

of the shape and density of microparticles on their margination propensity has been investigated. The number n of particles marginating and adhering onto the substrate of the chamber has been measured over time showing that: (i) the number of quasi-hemispherical silicon particles marginating towards the surface decreases with the shear rate S following a power law S^{-1}, regardless of their density and size; (ii) the number of marginating spherical silica particles decreases with the shear rate S with the scaling law $S^{-0.63}$; (iii) the number of marginating discoidal polysilicon particles decreases with the shear rate S with the scaling law $S^{-0.85}$. When comparing particles with similar weight, discoidal particles exhibit a higher margination propensity compared to quasi-hemispherical and spherical particles. As expected in a gravitational field, at a given shear rate (iv) large density particles marginate more than small density ones and (v) large particles marginate more than small ones.

These results may be of importance in the design of particles to be used for the systemic delivery of drugs or in biomedical imaging. In such applications, in fact, a marginating particle would have the ability of sensing the vessel walls for biological and biophysical diversities, such as the overexpression of specific antigens or the presence of openings and fenestrations, thus increasing the likelihood of recognizing the specific vascular or extravascular biological target.

Conflict of interest statement

This is to certify that none of the authors have any significant financial interest that would reasonably appear to be affected by the publication of this paper or that may have inappropriately influenced their work.

References

Choi, Y.S., Thomas, T., Kotlyar, A., Islam, M.T., Baker, J.R., 2005. Synthesis and functional evaluation of DNA-assembled polyamidoamine dendrimer clusters for cancer cell-specific targeting. Chemistry & Biology 12.

Cohen, M.H., Melnik, K., Boiarski, A.A., Ferrari, M., Martin, F.J., 2003. Microfabrication of silicon-based nanoporous particulates for medical applications. Biomedical Microdevices 5, 253–259.

Crommelin, D.J.A., Schreier, H., 1994. Liposomes. In: Kreuter, J. (Ed.), Colloidal Drug Delivery Systems. Marcel Dekker Inc., New York.

Decuzzi, P., Ferrari, M., 2006. The adhesive strength of non-spherical particles mediated by specific interactions. Biomaterials 27 (30), 5307–5314.

Decuzzi, P., Lee, S., Bhushan, B., Ferrari, M., 2005. Theoretical model for the margination of particles within blood vessels. Annals of Biomedical Engineering 32 (6), 793–802.

di Tomaso, E., Capen, D., Haskell, A., Hart, J., Logie, J.J., Jain, R.K., et al., 2005. Mosaic tumor vessels: cellular basis and ultrastructure of focal regions lacking endothelial cell markers. Cancer Research 65 (13), 5740–5749.

Duncan, R., 2003. The dawning era of polymer therapeutics. Nature Reviews: Drug Discovery 2, 347–360.

Ferrari, M., 2005a. Nanovector therapeutics. Current Opinion in Chemical Biology 9 (4), 343–346.

Ferrari, M., 2005b. Cancer nanotechnology: opportunities and challenges. Nature Reviews: Cancer 5 (3), 161–171.

Gavze, E., Shapiro, M., 1998. Motion of inertial spheroidal particles in a shear flow near a solid wall with special application to aerosol transport in microgravity. Journal of Fluid Mechanics 371, 59–79.

Goldman, A.J., Cox, R.G., Brenner, H., 1967. Slow viscous motion of a sphere parallel to a plane wall. II. Couette flow. Chemical Engineering Science 22, 653.

Goldsmith, H.L., Spain, S., 1984. Margination of leukocytes in blood flow through small tubes. Microvascular Research 27 (2), 204–222.

Gopalan, P.K., Smith, C.W., Lu, H., Berg, E.L., McIntire, L.V., Simon, S.I., 1997. Neutrophil CD18-dependent arrest on intercellular adhesion molecule 1 (ICAM-1) in shear flow can be activated through L-selectin. Journal of Immunology 158 (1), 367–375.

Hogg, A.J., 1994. Inertial migration of a non-neutrally buoyant particle in a two-dimensional shear flow. Journal of Fluid Mechanics 272, 285–318.

LaVan, D.A., Mcguire, T., Langer, R., 2003. Small-scale systems for in vivo drug delivery. Nature Biotechnology 21 (10), 1184–1191.

Lee, S.Y., Decuzzi, P., 2008. Analysis of the hydrodynamics forces on non-spherical particles within a capillary flow, internal communication.

MatLab 6.5, 2002. Image Processing Toolbox, The MAthWorks, Inc., Copyright 1984–2002.

Neri, D., Bicknell, R., 2005. Tumour vascular targeting. Nature Reviews Cancer 5, 436–446.

Pozrikidis, C., 2006. Flipping of an adherent blood platelet over a substrate. Journal of Fluid Mechanics 568, 161–172.

Rolland, J.P., Maynor, B.W., Euliss, L.E., Exner, A.E., Denison, G.M., DeSimone, J.M., 2005. Direct fabrication and harvesting of monodisperse, shape specific nano-biomaterials. Journal of American Chemical Society 127, 10096–10100.

Shinde Patil, V.R., Campbell, C.J., Yun, Y.H., Slack, S.M., Goetz, D.J., 2001. Particle diameter influences adhesion under flow. Biophysical Journal 80 (4), 1733–1743.

van Dillen, T., van Blaaderen, A., Polman, A., 2004. Ion beam shaping of colloidal assemblies. Materials Today, 40–46.

Wolfram, S., 2003. The Mathematica Book, fifth ed. Wolfram Media, Cambridge University Press, Cambridge.